Since January 2020 Elsevier has created a COVID-19 resource centre with free information in English and Mandarin on the novel coronavirus COVID-19. The COVID-19 resource centre is hosted on Elsevier Connect, the company's public news and information website.

Carbon 194 (2022) 34–41

Contents lists available at ScienceDirect

Carbon

journal homepage: www.elsevier.com/locate/carbon

3D-printed graphene polylactic acid devices resistant to SARS-CoV-2: Sunlight-mediated sterilization of additive manufactured objects

Flavio De Maio [a, b, 1], Enrico Rosa [c, 1], Giordano Perini [c, d], Alberto Augello [c, d], Benedetta Niccolini [c, d], Francesca Ciaiola [c], Giulia Santarelli [b], Francesca Sciandra [e], Manuela Bozzi [f], Maurizio Sanguinetti [a, b], Michela Sali [a, b], Marco De Spirito [c, d], Giovanni Delogu [b, g], Valentina Palmieri [c, d, h, *], Massimiliano Papi [c, d, **]

[a] Dipartimento di Scienze di Laboratorio e Infettivologiche, Fondazione Policlinico Universitario "A. Gemelli" IRCSS, Largo A. Gemelli, 8 00168, Rome, Italy
[b] Dipartimento di Scienze biotecnologiche di base, cliniche intensivologiche e perioperatorie – Sezione di Microbiologia, Università Cattolica del Sacro Cuore, Rome, Largo Francesco Vito 1, 00168, Italy
[c] Dipartimento di Neuroscienze, Università Cattolica del Sacro Cuore, Rome, Largo Francesco Vito 1, 00168, Italy
[d] Fondazione Policlinico Universitario "A. Gemelli" IRCSS, Largo A. Gemelli, 8 00168, Rome, Italy
[e] Istituto di Scienze e Tecnologie Chimiche "Giulio Natta", (SCITEC)-CNR, Roma, Italy
[f] Dipartimento di Scienze Biotecnologiche di Base, Cliniche Intensivologiche e Perioperatorie, Sezione di Biochimica e Biochimica Clinica, Università Cattolica del Sacro Cuore, Rome, Italy
[g] Mater Olbia Hospital, Olbia, Italy
[h] Istituto dei Sistemi Complessi, CNR, Via dei Taurini 19, 00185, Rome, Italy

ARTICLE INFO

Article history:
Received 1 January 2022
Received in revised form
21 February 2022
Accepted 14 March 2022
Available online 16 March 2022

Keywords:
Graphene
Scaffolds
SARS-CoV-2 inhibition
Nanotechnology
NIR light Sterilization

ABSTRACT

Additive manufacturing has played a crucial role in the COVID-19 global emergency allowing for rapid production of medical devices, indispensable tools for hospitals, or personal protection equipment. However, medical devices, especially in nosocomial environments, represent high touch surfaces prone to viral infection and currently used filaments for 3D printing can't inhibit transmission of virus [1].

Graphene-family materials are capable of reinforcing mechanical, optical and thermal properties of 3D printed constructs. In particular, graphene can adsorb near-infrared light with high efficiency. Here we demonstrate that the addition of graphene nanoplatelets to PLA filaments (PLA-G) allows the creation of 3D-printed devices that can be sterilized by near-infrared light exposure at power density analog to sunlight. This method has been used to kill SARS-CoV-2 viral particles on the surface of 3D printed PLA-G by 3 min of exposure. 3D-printed PLA-G is highly biocompatible and can represent the ideal material for the production of sterilizable personal protective equipment and daily life objects intended for multiple users.

1. Introduction

Tridimensional (3D) manufacturing has played a pivotal role in fighting the Coronavirus disease (COVID-19) pandemic with innovatively designed products developed through the collaboration between health professionals, engineers and creatives [1]. Examples of 3D-printed solutions established during the pandemic include valves for non-invasive ventilation respiratory supports, face shields, door handles, and COVID-19 lattice test swabs [1–3]. To achieve the best fit, the protective equipment has been produced using additive manufacturing combined after surface scanning of health workers' bodies. 3D printing comprises techniques of stereolithography, selective laser sintering, and fused deposition modeling [4]. Undoubtedly, desktop 3D printers based on fused deposition modeling and melted thermoplastics, are the most accessible and low-cost additive manufacturing technique [4].

Thermoplastic polymers (TP) are the most frequently utilized materials in additive manufacturing due to their low cost and low

* Corresponding author. Istituto dei Sistemi Complessi CNR, Via dei Taurini 19, 00185, Italy.
** Corresponding author. Dipartimento di Neuroscienze, Università Cattolica del Sacro Cuore, Rome, Largo Francesco Vito 1, 00168, Italy.
E-mail addresses: valentina.palmieri@cnr.it (V. Palmieri), massimiliano.papi@unicatt.it (M. Papi).
[1] Co-first authors.

https://doi.org/10.1016/j.carbon.2022.03.036
0008-6223/

melting temperatures. TP include acrylonitrile butadiene styrene (ABS), polylactic acid (PLA), polycarbonate (PC), and polyether ether ketone (PEEK) [5].

Among these, PLA has generated significant interest for medical applications for its biocompatibility and biodegradability [6]. PLA is the most used plastic in 3D printing since melts easily compared to many fossil-based plastics and thus it is easier to print and better suited for parts with complex or fine details. PLA is also one of the most environmentally friendly 3D printing materials and therefore a promising biopolymer for medical research, capable of substituting conventional petroleum-based polymers due to recyclability and compostability. PLA degrades via hydrolysis to lactic acid, depending on pH, temperature, autocatalytic behavior, and degree of water contact.

In addition, PLA can be processed with various additive manufacturing methods [7]. Some drawbacks limit its use in medical device production, such as brittleness, poor thermal stability, low elongation at break and impact strength, and low heat-distortion temperature [8].

To improve PLA thermal and electrical conductivity, and mechanical strength, additives such as cellulose, metals and carbon nanoparticles have been experimented [8].

Among nanomaterials, graphene is a promising technology in the biomedical field due to several advantages. Graphene, a widely studied bidimensional carbon nanomaterial, and its derivatives possess pro-differentiating effects on eukaryotic cells (such as stimulation of bone/muscle tissue growth on 3D scaffolds [9–11]), and antibacterial properties even towards antibiotic-resistant species [12–14]. Graphene has indeed high interaction with the microbial surface and can exert both a bacteriostatic and bactericidal effect according to the damages that hydrophobic areas induce in bacterial outer membrane [15].

Graphene-family materials are also capable of reinforcing mechanical, optical, and thermal properties of 3D printed constructs even in a small amount [16,17]. These improvements, of great importance to produce many medical devices, can therefore be obtained at extremely low costs with low toxicity, making it an easy-to-implement strategy.

Several uses of graphene have been proposed during COVID-19 emergency: graphene field-effect transistor has been proposed for the development of a Severe Acute Respiratory Syndrome Coronavirus (SARS-CoV-2) diagnostic device [18], but also sensors and wearable [19,20].

Our group has demonstrated that graphene can inhibit the infectivity of SARS-CoV-2 if embedded in textiles [19,21] and that graphene oxide can trap and induce precipitation of viral particles in solution. It has been also recently demonstrated an interaction between graphene and SARS-CoV-2 surface proteins [22].

One of the most noteworthy features of graphene is its strong interaction with light: a single layer of graphene (<0.5 nm of thickness) can absorb 2.3% of incident visible light [23]. This property is essential for photothermal therapies (PTT) as well as wound healing, muscle repair and angiogenesis, for regenerative medicine. NIR absorbers like graphene are used for the hyperthermic killing of cancer cells and microbial species due to hyperthermic effects [24]. Furthermore, graphene and its derivatives are easily added to thermoplastic polymers for 3D printing, making this technology easily implementable in laboratories.

Given these advantages, in this work, we investigate the feasibility of adding graphene nanoparticles to PLA filaments (PLA-G) for the creation of sterilizable objects intended for healthcare applications. PLA-G filaments, containing graphene in a range from 0.5% up to 5%, have been tested for (i) mechanical strength, (ii) near-infrared adsorption and thermal properties, and (iii) anti-SARS-CoV-2 properties. All the concentrations had high biocompatibility when eukaryotic cells have been grown on PLA-G surfaces. Using NIR light with power intensity analog to sunlight, we demonstrate the feasibility of using PLA-G for protective equipment production. Besides the intrinsic graphene inhibition of SARS-CoV-2 attachment, viral particles that might come in contact with PLA-G can be easily killed by sunlight, offering an economic and environmentally sustainable method for surface sterilization. This nanotechnology-based system can greatly impact the production of face masks, surgical instruments, and daily objects in healthcare or other working or public environments, such as schools or public transport.

2. Materials and methods

2.1. PLA-G filaments and 3D printing

PLA filaments containing G+ (Directa Plus) with different amounts of G+ flakes (0%, 0.5%, 2%, 5%) have been used. G+ was produced according to a proprietary patented technology involving three steps: expansion, exfoliation, and drying [25]. In Table S1, the main features of G+ are summarized. Full characterization of this nanomaterial is reported elsewhere [26]. The structure of 3D printed scaffolds was designed using modeled using 3D computer graphics and computer-aided design (CAD) software Rhinoceros software (Robert McNeel & Associates). Ultimaker S3 3D printer was used to produce 3D printed structures using a nozzle extruded at temperature of 180 °C and printing velocity of 20 mm/s. The nozzle diameter was 400 μm, and the thickness of a single layer was set to 200 μm. Shapes printed for different tests are resumed in Table S2 and Fig. S1.

2.2. Scanning electron microscopy (SEM)

SEM was performed to evaluate 3D printed material structure. All the samples were sputter-coated with platinum. Micrographies have been acquired with SEM Supra 25 (Zeiss, Germany) at several magnifications (scale bar are reported on each image). Images were analyzed using FIJI software (National Institute of Health, Bethesda, MD, USA).

2.3. Atomic force microscopy (AFM)

AFM was performed with a NanoWizard II (JPK Instruments AG, Berlin, Germany). The images were acquired using silicon cantilevers with high aspect-ratio conical silicon tips (CSC37 Mikro-Masch, Tallinn, Estonia) characterized by an end radius of about 10 nm, a half conical angle of 20°, and a spring constant of 0.6 N/m. Small scan areas (5 × 5 μm) were imaged. The surface roughness of all samples was evaluated by using the software JPK SPM Data Processing. Briefly, 3 scan areas were imaged with AFM for each sample. Then, the roughness was measured in terms of both arithmetical mean deviation of the assessed profile (Ra) and of root mean squared (Rq). The average Ra and Rq for each sample ± standard deviation were reported.

2.4. Mechanical testing of 3D printed PLA-G

Tensile strength (TS), elongation at break (EB), and elastic modulus (EM) were measured according to previous studies [27] using 3D printed dog-bone-shaped specimens or cylinders with a mechanical analyzer (UniVert CellScale system, Germany). The grip separation was 20 mm and the speed rate of 1 mm/s until breaking. At least three samples for each condition were used.

2.5. Cell cultures

African green monkey kidney (VERO) epithelial cells (ATCC CCL-81) were cultured in Dulbecco's Modified Eagle's Medium (DMEM) supplemented with 10% inactivated fetal calf serum (FCS) (Euro-Clone, Milan, Italy), 1% glutamine (EuroClone, Milan, Italy), 1% streptomycin - penicillin antibiotics (EuroClone, Milan, Italy) and incubated in a humidified atmosphere (5% CO2 at 37 °C). Cells were washed with sterile warm phosphate-buffered saline (PBS), trypsinized and counted, before replating in 48-well plates (Wuxi NEST Biotechnology Co., Ltd, China) at 7 x 10^4 cells/mL in the previously mentioned medium. Cells were infected with SARS-CoV-2 virus when >90% confluent monolayer was observed comprising approximately 1 x 10^6 cells/well after 72 h [28]. Murine myoblast C2C12 cells were purchased from the American Type Culture Collection (ATCC). Cells were maintained in DMEM medium (Sigma-Aldrich) supplemented with 10% fetal bovine serum (FBS, EuroClone), 2% penicillin-streptomycin (Sigma-Aldrich) at 37 °C in 5% CO_2. Two days after starting culture of C2C12 myoblasts, the medium was changed to differentiation medium (DM), which consists of DMEM, 2% Horse Serum (HS), 100 U/mL penicillin, and 100 μg/mL streptomycin and incubated from day 2 to day 6 to induce myotubes formation [29].

Human adenocarcinomic alveolar basal epithelial cells (A549) were purchased from American Type Culture Collection (ATCC). Cells were maintained in DMEM medium (Sigma-Aldrich) supplemented with 10% foetal bovine serum (FBS, EuroClone), 2% penicillin-streptomycin (Sigma-Aldrich), and 2% L-glutamine (Sigma-Aldrich). Cells were cultivated in T75 flasks and kept at 37 °C in 5% CO_2 humidity.

2.6. Toxicity assays and confocal microscopy

To investigate toxicity of PLA and PLA-G filaments, VERO and C2C12 cells were cultured on PLA or PLA-G supports and viability was assessed after 24 and 72 h. Cells were cultured on PLA or PLA-G supports in growth medium consisting of DMEM, 10% FBS, 100 U/mL penicillin, and 100 μg/mL streptomycin at 37 °C in of 5% CO_2. VERO cells were grown and plated as previously described [30]. Cell viability was assessed by using CellTiter-Glo® Luminescent Cell Viability Assay (Promega, Madison, WI, USA) according to manufacturer's instructions. Measurements, in triplicates, were performed using a multiplate reader (Cytation 3, Biotek, USA). Results were finally normalized to control (PLA blocks). For confocal imaging, cells were washed twice in 2 mL PBS per well, fixed (3.7% paraformaldehyde), permeabilized (Triton X-100, Fisher, 1:500) as previously reported [31]. Cells were stained using f-actin molecular probe rhodamine phalloidin (1:200; Life Technologies, Molecular Probes). Dapi nuclear stain (1:2000; Life Technologies, Molecular Probes) was used to stain nuclei. Rhodamine phalloidin was excited at 540 nm and emitted at 565 nm. DAPI was excited at 358 nm and emitted at 461 nm. Microscopy images were captured on a Nikon microscope (20X). Images were analyzed using FIJI software (National Institute of Health, Bethesda, MD, USA).

2.7. Effects of PLA and PLA-G surfaces on SARS-CoV-2

The antiviral effects of PLA or PLA-G were evaluated following ISO18184 procedures using VERO cells. SARS-CoV-2 can be cultivated in various cell lines that express the angiotensin converting enzyme 2 (ACE2) receptor, which is required for viral entry. The monkey kidney cell lines Vero-CCL81 and Vero E6 are most commonly used, and viral cytopathic effect (CPE) is often observed within 3 days of inoculation [32,33]. Briefly, 0.1 mL of PBS containing SARS-CoV-2 virus ($\approx 10^5$ viral particles/ml) was put on the surface of a 1 × 1 cm^2 3D printed sample. Materials were incubated 2 h at 37 °C, or 55 °C and 85 °C to simulate sunlight irradiation. After incubation, each material was placed in a new tube containing 5 mL of DMEM supplemented with 2% inactivated FCS, 1% glutamine, 1% streptomycin - penicillin antibiotics. Additionally, 0.1 mL of DMEM was used to wash and collect infection solutions in the wells containing the materials. Each tube containing infected material was vigorously vortexed five times, and 0.1 mL of suspension was used to infect VERO cells. The cytopathic effect was monitored daily by visual inspection and quantified by imaging after crystal violet staining using Cytation 3 (BIOTEK, USA). Images have been analyzed using the freely available ImageJ version 1.47v (NIH, USA). Every set of images corresponding to crystal violet staining was analyzed using the "Process > Batch > Macro tool" with the following steps: conversion to 8-bit, manual thresholding to convert image in binary and obtain the area covered by cells, smoothing and conversion to mask, and measurement of area.

2.8. Near infrared (NIR) light adsorption of PLA and antiviral effects evaluation

To assess the photothermal effect of 3D printed materials, dry samples were irradiated under an 808 nm laser diode (Laser Ever, China) for different time spans at a power density of 0.1 or 0.07 W cm^{-2} to obtain the same thermal effect of sunlight in a theoretical or measured summer day [34]. A thermal imaging camera (Xi400, Optris) was used to record the sample temperature. All tests were performed in triplicate.

2.9. Statistical analysis

All experiments were replicated at least three times. Microsoft Excel (2010) and Prism8 software (GraphPad) were used to compile and analyze data. All data were expressed as mean with SD and analyzed by one-way ANOVA comparison tests followed by Tukey's correction.

3. Results and discussion

COVID-19 pandemic has prompted the use of PLA and other thermoplastic-based printing filaments to produce PPE, medical devices, and daily life objects. PLA filaments composition can be modified with carbon nanomaterials such as bidimensional graphene, to improve the performance of 3D-printed medical devices. Indeed, the bare PLA filaments can lack the strength to produce fully functioning engineering parts, restricting the adoption of 3D technology [5].

In Fig. 1A, representative SEM images of 3D printed structures made of PLA or PLA-G with different graphene nanoplatelets concentrations (0.5%, 2%, or 5%) are shown. Graphene nanoplatelets used in this study have an average lateral dimension of 3 μm and a layer number comprised between 4 and 6 layers, as resumed in Table S1. The structures shown in Fig. 1A have been produced with a deposition speed of 20 mm/s and nozzle diameter of 0.4 mm using the Ultimaker S3 3D printer. Since the presence of graphene can alter the printing process and consequently the diameter of filaments, the quantification of this parameter obtained from SEM has been performed (Fig. S2). Overall, the presence of G nanoplatelets in the PLA filaments doesn't alter the printed structure significantly, as shown by SEM. Nanoscale roughness has been quantified from AFM imaging (Fig. S3) with an evident increase of surface roughness as graphene percentage goes from 0.5% to 5%. The increase of amount of G changes PLA viscosity and melting point causing a faster polymer solidification and a slower polymer relaxation after 3D-printing [35]. This thermodynamic behavior, during post-

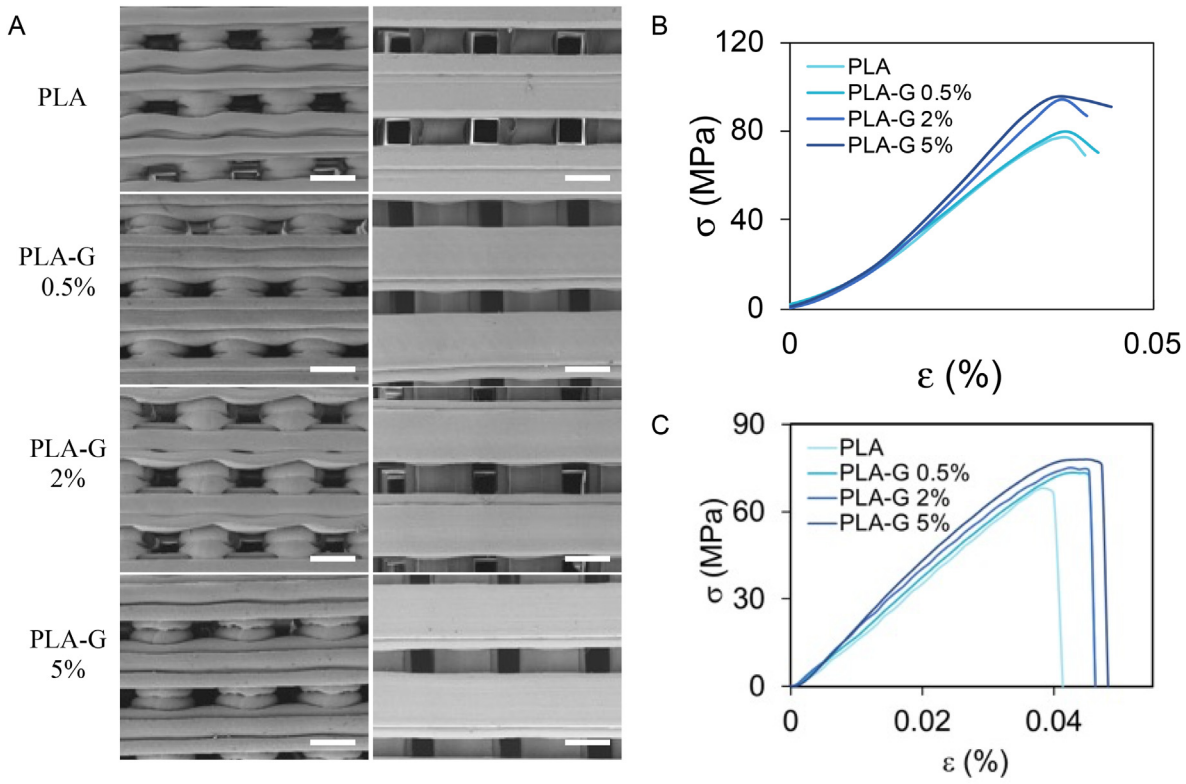

Fig. 1. Characterization of 3D printed structures by SEM imaging and mechanical analysis (A) Lateral and top views of PLA, PLA-G 0.5%, PLA-G 2% and PLA-G 5% discs by SEM, scale bar is 0.5 mm. Curves for compressive (B) and tensile (C) tests on PLA, PLA-G 0.5%, PLA-G 2% and PLA-G 5%.

printing solidification, increases the local roughness of the surfaces as the graphene concentration increases.

PLA and PLA-G have very similar hydrophobicity as measured by contact angle experiments (Fig. S3). Data reported in the literature report contact angles for PLA and graphene between 70° and 90°. This value can change due to several factors like the specific polymer preparation, the number of graphene layers, temperature, humidity etc. [36,37].

Curves obtained from compressive and tensile tests are shown in Fig. 1B and C, respectively. In Table 1, the results of tensile tests of 3D printed dogbones of PLA with or without graphene are shown. In Table 2 the results of compression tests on PLA and PLA-G cylinders are shown. The addition of G in the filaments increases the tensile and compression elastic modules up to 35% in compression and 20% in elongation using G at 5% in PLA-G (Table 1). The elongation at break increases up to 17.5%, the max stress in tension increases up to 13% and the yield stress up to 24%.

The mechanical properties of medical devices that are put under physical stress like ventilator valves or connectors for breathing devices are exceptionally important. Indeed, the device must be sufficiently strong to retain its integrity under conditions of normal wear and tear. Biocompatibility assessment is fundamental for devices intended for in vivo use. Biocompatibility of PLA and PLA-G

Table 1
Results of mechanical characterization after tensile tests of PLA and PLA-G samples.

	Stress max (Mpa)	%break	E (Gpa)
PLA	69	4.00%	2.9
PLA-G 0.5%	73	4.50%	3
PLA-G 2%	74	4.60%	3.2
PLA-G 5%	78	4.70%	3.5

Table 2
Results of mechanical characterization after compression tests of PLA and PLA-G samples.

	Yield stress (Mpa)	E (Gpa)
PLA	76	2.6 ± 0.2
PLA-G 0.5%	80	2.6 ± 0.2
PLA-G 2%	94	3.2 ± 0.26
PLA-G 5%	96	3.5 ± 0.28

was evaluated on VERO, C2C12 and A549 cells plated on 3D printed supports after 24 h of growth (Fig. 2A). Cell viability assays did not show any significant cell growth inhibition even at the highest concentration of G tested (PLA-G 5%). As highlighted from representative images of C2C12 cells grown on PLA-G 5% reported in Fig. 2B, cells were attached and grew easily on supports. Biocompatibility is maintained in these cells even after several days of growth (Fig. S4).

To assess the ability of PLA-G to capture SARS-CoV-2, a solution of SARS-CoV-2 containing ~10^5 viral particles/mL was let to interact with PLA and PLA-G supports (discs) for 2 h at 37 °C. Following incubation, contaminated discs were harvested and the plastic surface exposed to the SARS-CoV-2 containing solution washed. Discs and washing solution were recovered in 5 mL of sterile fresh medium and an aliquot of this suspension was used to infect VERO cells to measure viral infectivity (Fig. 3A). Representative images of infected VERO cells are shown in Fig. 3B: exposure of SARS-CoV-2 containing solution, even at the lowest concentration of graphene tested (PLA-G 0.5%), significantly reduced viral infectivity. Reduction in viral infectivity was proportional to the concentration of G in the PLA filaments, reaching a maximum with PLA-G 5%, supporting previous findings indicating the ability of G to bind and “trap” viral

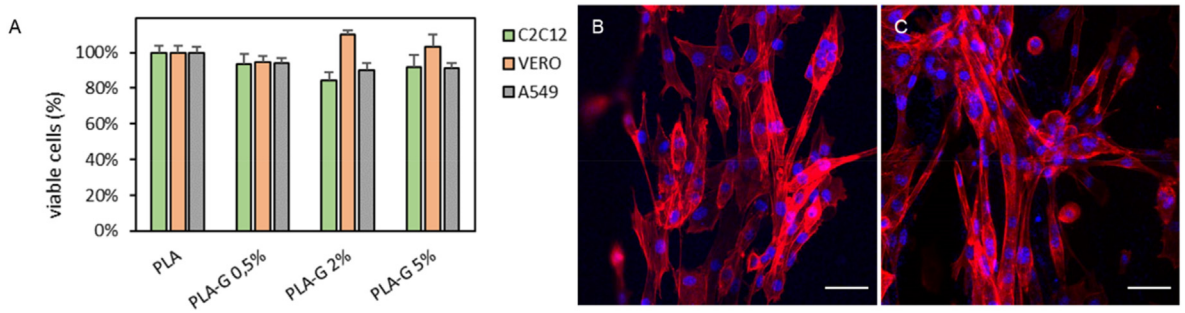

Fig. 2. Cell viability analysis on PLA supports (A) Viability of C2C12, VERO and A549 cells grown on PLA or PLA-G samples quantified by luminescence after 24 h. Representative confocal microscopy Z projection of C2C12 cells on PLA (B) and PLA-G 5% (C) with nuclei in blue (DAPI) and actin in red (rhodamine phalloidin). Scale bar is 50 μm.

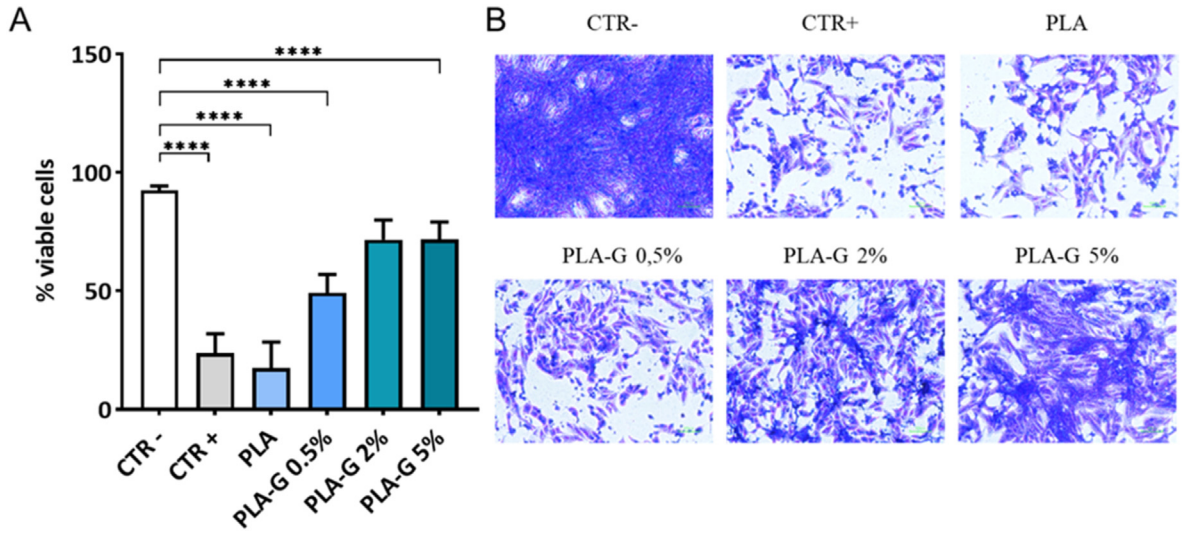

Fig. 3. Graphene functionalized PLA reduced infectivity of SARS-CoV-2. PLA and PLA-G (0.5%, 2.0% and 5%) functionalized PLA were incubated with a suspension of SARS-CoV-2 at the final concentration of ~10^5 viral particles/mL, for 2 h at 37 °C, to assess the ability to capture SARS-CoV-2 and subsequently reduce infectivity in VERO cells. Three days post-infection with solution recovered from surfaces, VERO cells were fixed and stained with crystal violet. Images were acquired using Cytation instrument an analyzed with ImageJ software and data were expressed as mean ± SD and analyzed by one-way ANOVA comparison tests followed by Tukey's correction. Asterisks indicate $p < 0{,}001$ (A). Representative images were obtained after crystal violet staining of VERO cells for each sample (B).

particles. However, we cannot exclude a detrimental effect of G on viruses' envelopes and consequent destabilization of the virions.

Graphene absorbs infrared light and has photocatalytic effects [38]. Since IR light occupies the largest proportion in the solar spectrum, we tested whether the graphene in the filaments could represent an easy and low-cost method to promote the adsorption of IR light by 3D printed constructs and consequently sterilize surfaces [38]. The photothermal catalytic disinfection experiment has been carried out under 808 nm laser light, the average temperature of the 3D structures has been monitored by a thermal camera. In Fig. 4, the results of temperature monitoring after exposure for 3 min of PLA and PLA-G samples are reported. In Fig. 4A, the illumination of samples with a NIR light having a power density of 0,07 W cm^{-2}, which corresponds to the measured average exposure of sunlight, causes an increase of temperature up to 50 °C with no marked differences between samples. On the contrary, when using the average power density of summer light (i.e. 0,1 W cm^{-2}), PLA temperature does not significantly increases, whereas samples containing graphene nanoplatelets substantially increase in temperature reaching after 3 min, 60 °C, 70 °C and 80 °C for PLA-G 0.5%, PLA-G 2% and PLA-G 5%, respectively.

Fig. 4C shows a 3D printed connector for a breathing device made of PLA or PLA-G. These connectors have been irradiated with an average power density of 0,07 W cm^{-2}, and results obtained with thermal imaging are shown in Fig. 4D and Fig, 4E. Temperatures of devices during irradiation are shown in Fig. 4F where is demonstrated that PLA-G 5% temperature increases up to 50 °C using a power intensity analog to sunlight.

To mimic sunlight effects, a suspension of SARS-CoV-2 was incubated on the discs for 2 h and the surfaces were exposed to NIR light. The increase of temperature correlated with a significant drop in infectivity compared to physiological body temperature (BT in Fig. 5A). At 0.07 W cm^{-2} and 0,1 W cm^{-2}, the further increase of temperature ($\approx$55° and $\approx$85 °C, respectively) was able to reduce SARS-CoV-2 infectivity, maintaining cell viability up to values of the not infected cells. The killing efficiency for PLA-G 5% surfaces towards SARS CoV-2 is reported in Fig. 5B, ranging from 55.9% at BT to 91.4% at 0,1 W cm^{-2} which corresponds to 85 °C. Since SARS-CoV-2 is extremely sensitive to high temperature [39], the method we developed can be used to easily clean and efficiently sterilize the surfaces using power density as sunlight exposure.

4. Conclusions

In the context of the pandemic challenges facing humanity today, the 3D printing production of protective equipment and

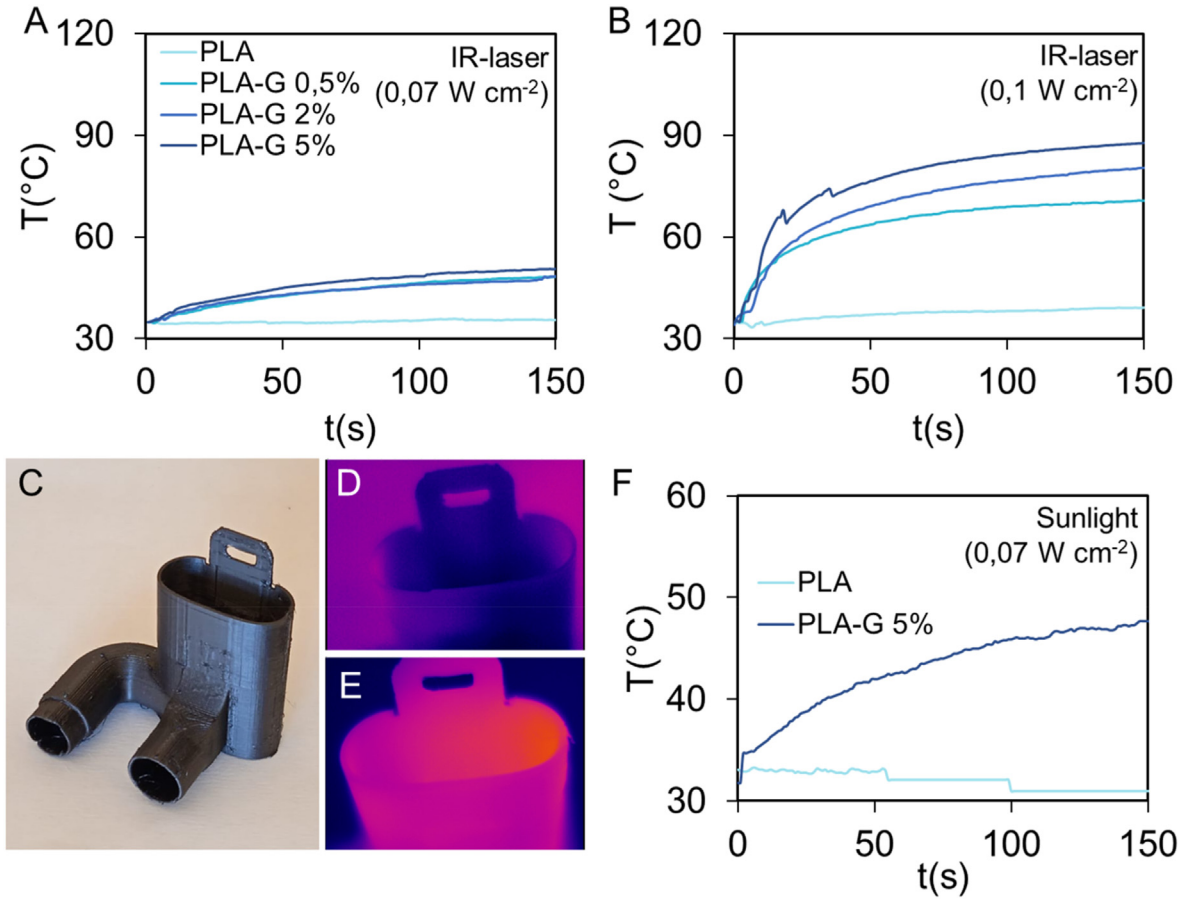

Fig. 4. Effects of exposure of PLA or PLA-G to 808 nm laser light at 0,07 W cm^{-2} (A), 0,1 W cm^{-2}(B). 3D printed connector for breathing device (C). Thermal images of 3D printed connector for breathing device in PLA (D) and PLA-G-5% (E) exposed for 150s to sunlight (about 0.07 W cm^{-2}) and the relative temperatures obtained by the thermal camera (F).

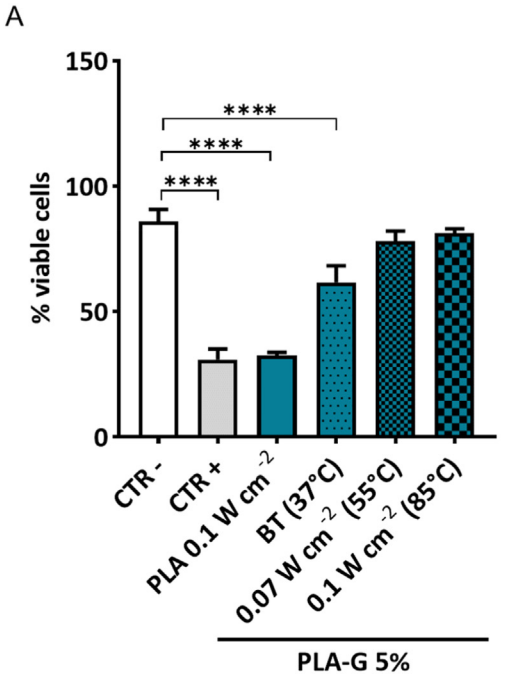

	% SARS-CoV-2 killed
PLA 0.1 W cm^{-2} (85°C)	2,9
PLA-G 5% BT (37°C)	55,9
PLA-G 5% 0.07 W cm^{-2} (55°C)	85,8
PLA-G 5% 0.1 W cm^{-2} (85°C)	91,4

Fig. 5. Effects of exposure to different NIR light of PLA and PLA-G-5% surfaces incubated with SARS-CoV-2 solutions. PLA and PLA-G 5% were incubated with a suspension of SARS-CoV-2 at the final concentration of ~10^5 viral particles/mL and exposed to different NIR light conditions (37 °C, 55 °C, 85 °C) for 2 h. Three days post-infection with solution recovered from surfaces, VERO cells were fixed and stained with crystal violet. Data are expressed as mean ± SD after analysis with ImageJ and analyzed by one-way ANOVA comparison tests followed by Tukey's correction. Asterisks indicate $p < 0,001$ (A). The ability to kill SARS-CoV-2 was quantified and significantly improved after NIR treatment as shown from the values in table (B).

more in general any surface that can readily warrant viral inactivation is of paramount importance. Traditionally, chemical disinfectants are the most widely used method to kill harmful pathogens, though the release of byproducts toxic for human health and the environment is a cause of major concern [38]. Nanotechnology has offered several approaches to cope with the COVID-19 emergency, as initially hypothesized in several papers [19,40]. Here we propose to exploit the photocatalytic properties of graphene nanoparticles embedded in the widely used biocompatible 3D-printable PLA. The most important feature, which differentiates graphene from many nanomaterials beside its mechanical and optical properties, is the interaction between graphene and different kind of microorganisms [13,41,42]. The use of 3 min of NIR (808 nm) with a power density of 0,1 W cm^{-2} allows killing SARS-CoV-2 deposited on surfaces using a light with intensity analog to sunlight. These results allow for extensive use of graphene PLA filaments, considering that exposure to sunlight can be a method to sterilize the surfaces of 3D printed objects. We also demonstrate that the mechanical behavior of the material is improved while the biocompatibility is retained toward eukaryotic cell lines. The World Health Organization highlighted the need for the prioritization of personal protective equipment supplies for frontline healthcare workers and PLA-G-based objects could represent the game-changer against pandemic spreading. Furthermore, NIR-mediated sterilization could represent a sustainable method to recycle medical devices and lower the impact on the environment [43,44]. The applications of PLA-G-based devices go beyond the nosocomial settings: with its high biocompatibility and mechanical resistance, PLA-G can become building material for high touch surfaces such as handles and buttons in public transport. Furthermore, 3D-printed SARS-CoV-2 can be used to produce long-term wearable prosthetic devices. Indeed the improvement of mechanical properties and the possibility to sterilize the surface by NIR could cope with the necessity, in the emergency setting, to reduce plaster and cast making. Indeed, given the hospital overflow together with the risk of transmission, protocols during pandemics could envisage the use of medical data files to send 3D-printed prosthetics to the patient directly at home [45]. Any PLA-G printed medical device could indeed be ordered remotely to reduce the hospitalizations and could be easily self-removed by the patient. Finally, 3D-printed air filters [46,47] made of PLA-G could be particularly useful for the possibility to use NIR light sterilization daily to maintain SARS-CoV-2 free air.

Funding

The work presented in this paper has been partially supported Università Cattolica del SC.

Credit author statement

F.D.M. Study design, experimental data analysis, writing original draft, statistical analysis.

E.R., G.O., A.A., B.N., F.V., G.S., F.S., M.B. experiments and experimental data analysis, figures.

M. Sanguinetti, M. Sali, M.D.S resources, administration.

G.D., V.P., M.P. data interpretation, writing, project coordination.

Declaration of competing interest

The authors declare that they have no known competing financial interests or personal relationships that could have appeared to influence the work reported in this paper.

Acknowledgment

We would like to acknowledge the contribution of 3D Bioprinting Research Core Facilty G-STeP and Microscopy Research Core Facilty G-STeP of the Fondazione Policlinico Universitario “A. Gemelli” IRCCS for sample processing.

Appendix A. Supplementary data

Supplementary data to this article can be found online at https://doi.org/10.1016/j.carbon.2022.03.036.

References

[1] R. Tino, R. Moore, S. Antoline, P. Ravi, N. Wake, C.N. Ionita, J.M. Morris, S.J. Decker, A. Sheikh, F.J. Rybicki, COVID-19 and the Role of 3D Printing in Medicine, 2020.
[2] B.I. Oladapo, S.O. Ismail, T.D. Afolalu, D.B. Olawade, M. Zahedi, Review on 3D printing: fight against COVID-19, Mater. Chem. Phys. 258 (2021) 123943.
[3] R. Perez-Mañanes, S.G.S. José, M. Desco-Menéndez, I. Sánchez-Arcilla, E. González-Fernández, J. Vaquero-Martín, J.P. González-Garzón, L. Mediavilla-Santos, D. Trapero-Moreno, J.A. Calvo-Haro, Application of 3D printing and distributed manufacturing during the first-wave of COVID-19 pandemic. Our experience at a third-level university hospital, 3D Print. Med. 7 (2021) 1–8.
[4] P. Ahangar, M.E. Cooke, M.H. Weber, D.H. Rosenzweig, Current biomedical applications of 3D printing and additive manufacturing, Appl. Sci. 9 (2019) 1713.
[5] A.N. Dickson, H.M. Abourayana, D.P. Dowling, 3D printing of fibre-reinforced thermoplastic composites using fused filament fabrication—a review, Polymers (Basel) 12 (2020) 2188.
[6] R.P. Rimington, A.J. Capel, S.D.R. Christie, M.P. Lewis, Biocompatible 3D printed polymers via fused deposition modelling direct C 2 C 12 cellular phenotype in vitro, Lab Chip 17 (2017) 2982–2993.
[7] R.A. Ilyas, S.M. Sapuan, M.M. Harussani, M. Hakimi, M.Z.M. Haziq, M.S.N. Atikah, M.R.M. Asyraf, M.R. Ishak, M.R. Razman, N.M. Nurazzi, Polylactic acid (PLA) biocomposite: processing, additive manufacturing and advanced applications, Polymers (Basel) 13 (2021) 1326.
[8] M. Bardot, M.D. Schulz, Biodegradable poly (lactic acid) nanocomposites for fused deposition modeling 3D printing, Nanomaterials 10 (2020) 2567.
[9] V. Palmieri, W. Lattanzi, G. Perini, A. Augello, M. Papi, M. De Spirito, 3D-printed graphene for bone reconstruction, 2D Mater (2020).
[10] V. Palmieri, F. Sciandra, M. Bozzi, M. De Spirito, M. Papi, 3D graphene scaffolds for skeletal muscle regeneration: future perspectives, Front. Bioeng. Biotechnol. 8 (2020).
[11] P. Bellet, M. Gasparotto, S. Pressi, A. Fortunato, G. Scapin, M. Mba, E. Menna, F. Filippini, Graphene-based scaffolds for regenerative medicine, Nanomaterials 11 (2021) 404.
[12] M. Papi, V. Palmieri, F. Bugli, M. De Spirito, M. Sanguinetti, C. Ciancico, M.C. Braidotti, S. Gentilini, L. Angelani, C. Conti, Biomimetic antimicrobial cloak by graphene-oxide agar hydrogel, Sci. Rep. 6 (2016), https://doi.org/10.1038/s41598-016-0010-7.
[13] V. Palmieri, M. Barba, L. Di Pietro, S. Gentilini, M.C. Braidotti, C. Ciancico, F. Bugli, G. Ciasca, R. Larciprete, W. Lattanzi, C. Conti, M. Papi, Reduction and shaping of graphene-oxide by laser-printing for controlled bone tissue regeneration and bacterial killing, 2D Mater 5 (2018), https://doi.org/10.1088/2053-1583/aa9ca7.
[14] A.M. Díez-Pascual, Antibacterial Action of Nanoparticle Loaded nanocomposites based on graphene and its derivatives: a mini-review, Int. J. Mol. Sci. 21 (2020) 3563.
[15] V. Palmieri, F. Bugli, M.C. Lauriola, M. Cacaci, R. Torelli, G. Ciasca, C. Conti, M. Sanguinetti, M. Papi, M. De Spirito, Bacteria meet graphene: modulation of graphene oxide nanosheet interaction with human pathogens for effective antimicrobial therapy, ACS Biomater. Sci. Eng. 3 (2017) 619–627.
[16] C.S.D. Cabral, S.P. Miguel, D. de Melo-Diogo, R.O. Louro, I.J. Correia, In situ green reduced graphene oxide functionalized 3D printed scaffolds for bone tissue regeneration, Carbon N. Y. 146 (2019) 513–523.
[17] H. Ma, C. Jiang, D. Zhai, Y. Luo, Y. Chen, F. Lv, Z. Yi, Y. Deng, J. Wang, J. Chang, A bifunctional biomaterial with photothermal effect for tumor therapy and bone regeneration, Adv. Funct. Mater. 26 (2016) 1197–1208.
[18] D. Kong, X. Wang, C. Gu, M. Guo, Y. Wang, Z. Ai, S. Zhang, Y. Chen, W. Liu, Y. Wu, Direct SARS-CoV-2 nucleic acid detection by Y-shaped DNA dual-probe transistor assay, J. Am. Chem. Soc. 143 (2021) 17004–17014.
[19] V. Palmieri, M. Papi, Can graphene take part in the fight against COVID-19? Nano Today (2020) 100883.
[20] S. Afroj, L. Britnell, T. Hasan, D. V Andreeva, K.S. Novoselov, N. Karim, Graphene-based Technologies for tackling COVID-19 and future pandemics, Adv. Funct. Mater. (2021) 2107407.
[21] F. De Maio, V. Palmieri, G. Babini, A. Augello, I. Palucci, G. Perini, A. Salustri, M. De Spirito, M. Sanguinetti, G. Delogu, L.G. Rizzi, G. Cesareo, P. Soon-Shiong, M. Sali, M. Papi, Graphene nanoplatelet and Graphene oxide functionalization

of face mask materials inhibits infectivity of trapped SARS-CoV-2, medRxiv (2020) 2020, https://doi.org/10.1101/2020.09.16.20194316, 09.16.20194316.
[22] M.A. Unal, F. Bayrakdar, H. Nazir, O. Besbinar, C. Gurcan, N. Lozano, L.M. Arellano, S. Yalcin, O. Panatli, D. Celik, Graphene oxide nanosheets interact and interfere with SARS-CoV-2 surface proteins and cell receptors to inhibit infectivity, Small 17 (2021) 2101483.
[23] V. Palmieri, M. De Spirito, M. Papi, Graphene-based scaffolds for tissue engineering and photothermal therapy, Nanomedicine 15 (2020) 1411–1417.
[24] A. Rosenkranz, G. Perini, J.Y. Aguilar-Hurtado, D.F. Zambrano, B. Wang, B. Niccolini, P. Henriques, E. Rosa, F. De Maio, G. Delogu, Laser-mediated antibacterial effects of few-and multi-layer Ti3C2Tx MXenes, Appl. Surf. Sci. (2021) 150795.
[25] L. Bonetti, A. Fiorati, A. Serafini, G. Masotti, F. Tana, A. D'Agostino, L. Draghi, L. Altomare, R. Chiesa, S. Farè, Graphene nanoplatelets composite membranes for thermal comfort enhancement in performance textiles, J. Appl. Polym. Sci. (n.d.) 49645.
[26] G. Cesareo, M.R. Parrini, L.G. Rizzi, Continuous Process for Preparing Pristine Graphene Nanoplatelets, 2020.
[27] L.J. Pérez-Córdoba, I.T. Norton, H.K. Batchelor, K. Gkatzionis, F. Spyropoulos, P.J.A. Sobral, Physico-chemical, antimicrobial and antioxidant properties of gelatin-chitosan based films loaded with nanoemulsions encapsulating active compounds, Food Hydrocolloids 79 (2018) 544–559.
[28] M. Siouda, A.D. Dujardin, L. Barbollat-Boutrand, M.A. Mendoza-Parra, B. Gibert, M. Ouzounova, J. Bouaoud, L. Tonon, M. Robert, J.-P. Foy, CDYL2 epigenetically regulates MIR124 to control NF-κB/STAT3-dependent breast cancer cell plasticity, iScience 23 (2020) 101141.
[29] P. Scotton, D. Bleckmann, M. Stebler, F. Sciandra, A. Brancaccio, T. Meier, J. Stetefeld, M.A. Ruegg, Activation of muscle-specific receptor tyrosine kinase and binding to dystroglycan are regulated by alternative mRNA splicing of agrin, J. Biol. Chem. 281 (2006) 36835–36845.
[30] M. Utsuyama, K. Hirokawa, C. Mancini, R. Brunelli, G. Leter, G. Doria, Differential effects of gonadectomy on thymic stromal cells in promoting T cell differentiation in mice, Mech. Ageing Dev. 81 (1995) 107–117.
[31] E.K. Krasnowska, E. Pittaluga, A.M. Brunati, R. Brunelli, G. Costa, M. De Spirito, A. Serafino, F. Ursini, T. Parasassi, N-acetyl-l-cysteine fosters inactivation and transfer to endolysosomes of c-Src, Free Radic. Biol. Med. 45 (2008) 1566–1572.
[32] S. Stelzer-Braid, G.J. Walker, A. Aggarwal, S.R. Isaacs, M. Yeang, Z. Naing, A.O. Stella, S.G. Turville, W.D. Rawlinson, Virus isolation of severe acute respiratory syndrome coronavirus 2 (SARS-CoV-2) for diagnostic and research purposes, Pathology 52 (2020) 760–763.
[33] M.J. Binnicker, Can testing predict SARS-CoV-2 infectivity? The potential for certain methods to be surrogates for replication-competent virus, J. Clin. Microbiol. 59 (2021), e00469-21.
[34] H. Shi, P.J. Sadler, How promising is phototherapy for cancer? Br. J. Cancer 123 (2020) 871–873.
[35] E. Stoleru, C. Vasile, A. Irimia, M. Brebu, Towards a bioactive food packaging: poly (lactic acid) surface functionalized by chitosan coating embedding clove and argan oils, Molecules 26 (2021) 4500.
[36] J. Li, F. Wang, Water graphene contact surface investigated by pairwise potentials from force-matching PAW-PBE with dispersion correction, J. Chem. Phys. 146 (2017) 54702.
[37] R. Raj, S.C. Maroo, E.N. Wang, Wettability of graphene, Nano Lett 13 (2013) 1509–1515.
[38] R. Zhang, C. Song, M. Kou, P. Yin, X. Jin, L. Wang, Y. Deng, B. Wang, D. Xia, P.K. Wong, Sterilization of Escherichia coli by photothermal synergy of WO3−x/C nanosheet under infrared light irradiation, Environ. Sci. Technol. 54 (2020) 3691–3701.
[39] A.W.H. Chin, J.T.S. Chu, M.R.A. Perera, K.P.Y. Hui, H.-L. Yen, M.C.W. Chan, M. Peiris, L.L.M. Poon, Stability of SARS-CoV-2 in different environmental conditions, The Lancet Microbe 1 (2020) e10.
[40] C. Weiss, M. Carriere, L. Fusco, I. Capua, J.A. Regla-Nava, M. Pasquali, J.A. Scott, F. Vitale, M.A. Unal, C. Mattevi, Toward nanotechnology-enabled approaches against the COVID-19 pandemic, ACS Nano (2020).
[41] V. Palmieri, F. Bugli, M. Cacaci, G. Perini, F. De Maio, G. Delogu, R. Torelli, C. Conti, M. Sanguinetti, M. De Spirito, R. Zanoni, M. Papi, Graphene oxide coatings prevent Candida albicans biofilm formation with a controlled release of curcumin-loaded nanocomposites, Nanomedicine 13 (2018) 2867–2879, https://doi.org/10.2217/nnm-2018-0183.
[42] F. De Maio, V. Palmieri, A. Salustri, G. Perini, M. Sanguinetti, M. De Spirito, G. Delogu, M. Papi, Graphene oxide prevents mycobacteria entry into macrophages through extracellular entrapment, Nanoscale Adv 1 (2019) 1421–1431, https://doi.org/10.1039/c8na00413g.
[43] V. Palmieri, F. De Maio, M. De Spirito, M. Papi, Face masks and nanotechnology: keep the blue side up, Nano Today 37 (2021) 101077, https://doi.org/10.1016/j.nantod.2021.101077.
[44] S. Feng, C. Shen, N. Xia, W. Song, M. Fan, B.J. Cowling, Rational use of face masks in the COVID-19 pandemic, Lancet Respir. Med. 8 (2020) 434–436.
[45] A. Sedigh, A.R. Kachooei, P.K. Beredjiklian, A.R. Vaccaro, M. Rivlin, Safety and efficacy of casting during COVID-19 pandemic: a comparison of the mechanical properties of polymers used for 3D printing to conventional materials used for the generation of orthopaedic orthoses, Arch. Bone Jt. Surg. 8 (2020) 281.
[46] R. Shaylor, M. Francis, E. Shaylor, S. Dadia, B. Cohen, Development and validation of a 3D printed antiviral ventilator filter-a comparative study, BMC Anesthesiol 21 (2021) 1–6.
[47] A. Aydin, Z. Demirtas, M. Ok, H. Erkus, G. Cebi, E. Uysal, O. Gunduz, C.B. Ustundag, 3D printing in the battle against COVID-19, Emergent Mater 4 (2021) 363–386.